Sensors and Materials, Vol. 29, No. 7 (2017) 1017–1023
MYU Tokyo

S & M 1393

Study of the Single-Point Laser 3D Footprint Detecting System at a Crime Scene

Nan Pan* and Lifeng Kan[1]

Aviation College, Kunming University of Science & Technology,
No. 727 Jingming South Road, Chenggong University Town, Kunming, 650500, P. R. China
[1]Faculty of Mechanical & Electrical Engineering, Kunming University of Science & Technology,
No. 727 Jingming South Road, Chenggong University Town, Kunming, 650500, P. R. China

(Received February 15, 2016; accepted February 28, 2017)

Keywords: 3D footprints, single-point laser, feature extraction, similarity comparison

Footprints found at a crime scene are very difficult to use to narrow the scope of identifying a suspect or to clarify the direction of an investigation. 3D scanning (microscopic), which could be more effective than 2D imaging in reflecting the detailed features of footprints, still involves high hardware costs and an exponential increase in calculation capacity owing to the large size of 3D files. To solve these problems, a single-point laser 3D footprint detecting system was designed and developed. The key technologies in this system, such as feature extraction and similarity comparison, are described in detail. Finally, the experiment results of 3D footprint inspection demonstrated the accuracy and reliability of this system.

1. Introduction

3D footprints can completely and fully reflect the outward structural morphology of the contact region of the foot with weight-bearing objects. They are an intuitive and comprehensive indicator of the usual habitual movements of a person.[1–3]

Conventional techniques of 3D footprint feature extraction are based on either plaster molding techniques or computational modeling of 3D surfaces. These approaches have several drawbacks, such as the lack of a uniform testing standard, heavy reliance on specialized equipment, and dependence on the professional experience of investigators.[4–6] The single-point laser displacement test method has important features, which induce not being damaging to the surface of the object, it is not impacted by ambient light, and it has high precision, small data files, and good frequency response, all of which are superior to other methods of measurement. It is very effective for the noncontact precision measurements of details of the trace line of a footprint.[7,8]

In this paper, a 3D footprint analysis system, which utilizes Wenglor high-performance laser ranging sensors to perform nondestructive measurements of collected samples, is proposed. This system can considerably improve the efficiency and effectiveness of footprint analyses conducted by junior inspectors.

*Corresponding author: e-mail: nanpan@kmust.edu.cn
http://dx.doi.org/10.18494/SAM.2017.1547

ISSN 0914-4935

2. Key Algorithms and Software Implementations

2.1 Measuring characteristic data

In accordance with relevant 3D footprint analysis theory, the footprint's centerline is taken as the *Y*-axis. Then, the origin *O* is determined by measuring 75 mm from the heel point along the *Y*-axis and marking the location. A vertical line is drawn through the origin *O* perpendicular to the *Y*-axis; this is the *X*-axis. These assignments are reflected on the software interface. After the system receives confirmation of the centerline and the heel point, it automatically generates the corresponding *X*-axis, *Y*-axis, and origin *O* on the footprint image according to the pulse pixel ratio.

2.1.1 Measurement of features of the forefoot and hallux regions

The forefoot area indentation height refers to uneven indentations reflected from the forefoot area. The hallux zone height refers to the uneven indentation reflected from the area of the big toe. The differences in the individual barefoot morphology combined with the difference in the magnitude and the distribution of force exerted while walking cause different forefoot and hallux indentations. The uneven pattern contains the latitude and longitude position differences of the *X*- and *Y*-axes, in addition to the difference observed in the base level on the *Z*-axis. The forefoot area and the hallux zone, a total of 23 coordinates, are measured by laser ranging sensors to determine the height along the *Z*-axis. A left footprint is used as an example (unit: mm). The 17 coordinates of the forefoot area are represented as follows: H0(0,120) peak point; H1(0,130), H2(10,130), H3(10,120), H4(10,110), H5(0,110), H6(−10,110), H7(−10,120), and H8(−10,130) are the side points; and H9(0,150), H10(20,140), H11(30,120), H12(30,90), H13(0,90), H14(−30,90), H15(−30,120), and H16(−30,150) are the bottom points. The hallux zone and its six points are h0(−30,150), h1(−30,170), h2(−10,170), h3(−10,150), h4(−10,130), and h5(−30,130). Note that h0 and H16 are overlapping points, as are h4 and H8. The coordinate system and coordinate locations are shown in Fig. 1(a).

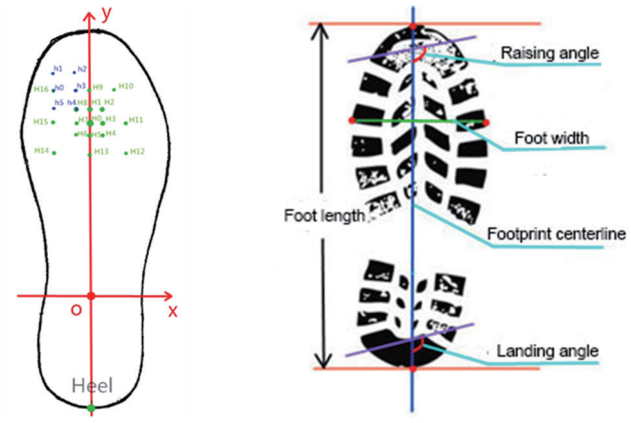

(a) (b)

Fig. 1. (Color online) (a) Footprint coordinate system and coordinate positioning and (b) landing angle, foot length, and foot width.

If we assume that the center point of the forefoot area has a height of H0 (unit: mm), then the *j*th bottom point and the side point heights are H_j and H_j', respecively. Let $g_j = H_0 - H_j$ and denote it as the full-slope gradient in the *j*th direction. Let $g_j' = H_0 - H_j'$ and denote it as the mid-slope gradient in the *j*th direction, where $j = 1, 2, \ldots, 8$. Similarly, set the height of the center toe region as h0 and the height of the peripheral regions as h_j, where $j = 1, 2, \ldots, 5$. Let $d_j = h_0 - h_j$ and denote it as the hallux-zone gradient in the *j*th direction. The motor drives the laser sensor to automatically measure the range of data of the 23 coordinates on the *Z*-axis. After calculating the full-slope gradient, mid-slope gradient, and hallux-zone gradient in all directions, these values are displayed on the front panel of the software; manual corrections of the outliers can then be carried out if anomalies in data points are observed.

2.1.2 Raising and landing angle, foot length, and foot width measurements

After measuring the forefoot area and the hallux-zone characteristics, the foot length, forefoot width, and the raising and landing angles are measured. As the heel point has already been selected, directly clicking on the tip of the toe determines the foot length. The width of the foot is measured by selecting the left and right points of the forefoot of the footprint image. The landing angle is measured by connecting the end points of the landing regions. The connection lines are drawn on the basis of experience. The angle that intersects the footprint centerline is the landing angle. The specifics are shown in Fig. 1(b).

2.2 Test analyses and database

Through multiple iterations of image acquisition and measurement, the footprint characteristics of the perpetrator and the suspects were determined. Footprint comparative analyses were then conducted. The full-slope gradient and mid-slope gradient of the crime scene footprint were denoted as g_{0j} and g_{0j}', respectively. The *i*th suspect footprint has a full-slope gradient g_{ij} and a mid-slope gradient g_{ij}'. The hallux-zone gradient of the crime scene footprint was expressed as d_{0j}. The *i*th suspect has a hallux-zone gradient expressed as d_{ij}. The definitions are as follows:

$$A_1{}^2 = \sum_{j=1}^{8} \left(g_{0j} - g_{ij}\right)^2, \tag{1}$$

$$A_2{}^2 = \sum_{j=1}^{8} \left(g_{0j}' - g_{ij}'\right)^2, \tag{2}$$

$$A_3{}^2 = \sum_{j=1}^{5} \left(d_{0j} - d_{ij}\right)^2. \tag{3}$$

In this expression, $A_1{}^2$ denotes the perpetrator and the forefoot indent of *i*th suspect's "sum of the difference between full-slope gradients squared" over all eight coordinates. This is abbreviated as "full-gradient sum". $A_2{}^2$ represents the "sum of the difference between mid-slope gradients squared" over all eight coordinates, abbreviated as "mid-gradient sum". $A_3{}^2$ indicates the "sum of

the difference between hallux-zone gradient squared", abbreviated as "hallux gradient sum". The absolute difference in the landing angle between the crime scene footprint and the suspect footprint is referred to as the "landing mark difference".

$$A_4 = |\alpha_0 - \alpha_i| \tag{4}$$

The absolute difference in the raising angle between the crime scene footprint and the suspect footprint is referred to as the "raising mark difference".

$$A_5 = |\beta_0 - \beta_i| \tag{5}$$

The absolute difference in the foot length between the crime scene footprint and the suspect footprint is referred to as the "foot length difference".

$$A_6 = |I_0 - I_i| \tag{6}$$

The absolute difference in the foot width between the crime scene footprint and the suspect footprint is referred to as the "forefoot width difference".

$$A_7 = |K_0 - K_i| \tag{7}$$

(1) Determination of threshold value

${A_1}^2$ and ${A_2}^2$ obey the χ^2 distribution with 8 degrees of freedom and the distribution with 5 degrees of freedom, respectively. According to Eq. (1):

$${A_1}^2 = \sum_{j=1}^{8} \frac{\left(g_{0j} - g_{ij}\right)^2}{2\sigma^2} - {\chi_8}^2. \tag{8}$$

For the selected value of α,

$$P\left({A_1}^2 > {\chi_8}^2(\alpha)\right) = \alpha, \tag{9}$$

which is

$$P\left[\sum_{j=1}^{8}\left(g_{0j} - g_{ij}\right)^2\right] > 2\sigma^2{\chi_8}^2\alpha = \alpha. \tag{10}$$

Thus, the threshold value of ${A_1}^2$ is $2\sigma^2{\chi_8}^2(\alpha)$, which can be determined, simply by selecting the value of α. The specific value of ${\chi_8}^2(\alpha)$ can also be determined by checking the distribution table. Then the specific threshold value of ${A_1}^2$ could be determined from the statistics of each sampling value of σ. Similarly, the threshold values of ${A_2}^2$, ${A_3}^2$, A_4, A_5, A_6, and A_7 can be calculated.

After a large number of experiments, the seven indicators of footprint characteristics were found to fall into a normal distribution. The threshold values could be determined for every

indicator via mathematical modeling and the utilization of experimental data. A comparative analysis of the experimental data and the threshold value can determine the maker of the footprint. Therefore, this method can be used to either confirm or reject a suspect. The seven indicator reference threshold values are listed in Table 1.

(2) Outline of the principle of footprint characteristic analysis

The seven key characteristics of 3D footprints, namely, the footprint length, forefoot width, raising angle, landing angle, full-gradient, mid-gradient, and hallux-gradient, were calculated accurately. If the subsequent values were less than or equal to the threshold values, we can conclude that the suspect's footprint and the crime scene footprint are similar in terms of the height characteristics. If one of the indicators was calculated to be greater than the threshold value, we can conclude that the suspect's footprint and the crime scene footprint are different in terms of the height characteristics.

3. Experimental Testing

On January 1, 1999, a murder was committed in a country lane near the eastern side of a city airport in Henan province. The victim was a primary school teacher, female, 23 years old. Crime scene examination extracted traces of sperm and 3D footprints as physical evidence. Forensic examination reported that the cause of death was stabbing through the heart by a dagger. Police investigators categorized this case as a rape–murder case with a single perpetrator. Despite considerable effort by police investigators, this case remained unsolved.

In March 2015, the extracted sperm DNA sample was matched to a local suspect X. After X was arrested, he named an accomplice; X confessed to the rape but named Li as the murderer. However, Li had died in 2007 and was therefore unable to corroborate this. The Supreme Court requested supplementary evidence for the integrity of the chain of evidence. To fulfill this request, the Municipal Public Security Bureau used the system described in this paper to compare the 3D footprint plaster model of the suspect X with the 3D footprint model collected at the crime scene. The analysis quickly showed that the right footprint indentation had the same height characteristics as those from the crime scene footprint. The analysis indicated that with the exception of the victim, the only footprints at the scene were left by Qiao. The reliability of the analyses was 98%. In combination with the other evidence left at the crime scene, this completed the chain of evidence. The crime scene and suspect's right footprint model are shown in Fig. 2. The crime scene right footprint model (No. 7-1) was compared with the suspect's left footprint sample (No. 7-2) to produce the results shown in Table 2. The crime scene right footprint model (No. 7-1) was compared with the suspect's right footprint sample (No. 7-3) to produce the results presented in Table 3.

Table 1
Seven indicators of variable difference theory.

Indicator reference	A_1^2	A_2^2	A_3^2	A_4	A_5	A_6	A_7
Threshold value	45	25	22	8	8	11	5.4
Reliable probability	All greater than or equal to 99%						

(a) (b) (c)

Fig. 2. (Color online) Right footprint model of crime scene: (a) No. 7-1 Sample model of suspect's footprint, (b) left model No. 7-2, and (c) right model No. 7-3.

Table 2
Test calculation of footprints Nos. 7-1 and 7-2.

Indicator	Full-gradient	Mid-gradient	Hallux-gradient	Landing angle	Raising angle	Foot length	Forefoot width
Value	40.8	18.0	17.6	3.63	6.41	6.08	2.54

Table 3
Test calculation of footprints Nos. 7-1 and 7-3.

Indicator	Full-gradient	Mid-gradient	Hallux-gradient	Landing angle	Raising angle	Foot length	Forefoot width
Value	37.5	12.2	14.9	1.27	2.23	6.64	3.02

4. Conclusions

A single-point laser 3D footprint detecting system was designed and developed using the LabVIEW platform. This system combined the precision of laser ranging sensors, computer control, and imaging technology to perform key functions such as image acquisition, footprint feature extraction, and comparative analyses. It has considerably supported the efforts of a police investigation by effectively narrowing down the range of possible suspects. Experimental results successfully demonstrated the effectiveness and accuracy of this system.

Acknowledgments

This study was supported by the key project of technology research program funded by the Key Science and Technology Project of Yunnan Province (No. 2016RA042) and the Key Science and Technology Project of Kunming City (No. 2015-1-S-00284).

References

1 J. L. Han: Trace Inspection (China Democracy and Rule of Law Press , Beijing, 2007).
2 L. Wang: Law Soc. **8** (2008) 165.
3 Y. H. Yang: J. Yunnan Police Officer Acad. **1** (2014) 103.
4 J. L. Han (ed): Footprint Inspection Technology (Chinese People's Public Security University Press, 2008).
5 L. M. Shi, S. Bi, and J. Z. Jiang: Criminal Technol. **5** (2004) 19.
6 W. Wang, C. Li, E. W Tollner, and G. C. Rains: Comput. Electr. Agriculture **84** (2012) 68.
7 F. Chen, P. T. Chen, P. Y. Zhu, and J. Gao: Meas. Control Technol. **33** (2014) 76.
8 M. Zeng, X. R. Yang, and G. Luo: J. Cent. South Univ. (Science and Technology) **34** (2003) 184.

About the Authors

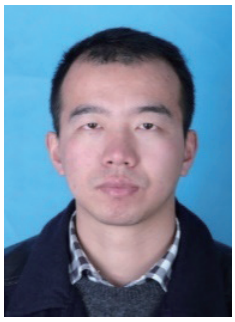

Nan Pan is from Huaiyuan, Anhui Province. He received his B.Sc. degree in 2008 from Anhui University of Science & Technology and his Ph.D. degree in 2012 from Kunming University of Science & Technology. He is now a lecturer and master instructor in Aviation College, Kunming University of Science & Technology. His main research interests include signal processing and criminal investigation special equipment R&D.

Lifeng Kan is from Linyi, Shandong Province. He received his B.Sc. degree in 2015 from Qingdao Technological University. He is now an M.Sc. student in Kunming University. His main research interests include signal processing and criminal investigation special equipment R&D.